Supplement of

Simulated reductions in Heterogeneous Isoprene Epoxydiol Reactive Uptake from aerosol morphology in the contiguous United States using the Community Multiscale Air Quality Model (CMAQv5.3.2)

Sara Farrell et al.

Correspondence to: Sara L. Farrell (slfarrel@live.unc.edu) and William Vizuete (vizuete@unc.edu)

S1. IEPOX Heterogeneous Reactive Uptake

In CMAQ, IEPOX reactive uptake has been parameterized by the following heterogeneous rate constant (Eddingsaas et al., 2010; Pye et al., 2013):

$$IEPOX_{(g)} \rightarrow IEPOXSOA_{(aerosol)} \quad \text{(S1)}$$

$$k_{het} = \frac{SA}{\frac{r_p}{D_g} + \frac{4}{\nu\gamma_{IEPOX}}} \quad \text{(S2)}$$

Where SA is the surface area of the aerosol that IEPOX partitions to, r_p is the aerosol particle radius, D_g is the gas-phase diffusion of IEPOX ($1.9 \times (M_{IEPOX})^{-2/3}$ m^2/s) where M_{IEPOX} is 118 g/mol, ν is the mean molecular speed of IEPOX ($\sqrt{8RT/\pi M_{IEPOX}}$), where R is the ideal gas constant (0.08206 L-atm/mol-K) and γ_{IEPOX} is the following reactive uptake probability coefficient (Eddingsaas et al., 2010; Gaston et al., 2014; Pye et al., 2013; Schmedding et al., 2019; Schmedding et al., 2020):

$$\frac{1}{\gamma_{IEPOX}} = \frac{1}{\alpha} + \frac{\upsilon * r_p^2}{4H_{inorg} * R * T * D_a * r_{core}} * \frac{1}{q * \coth(q) - \frac{1}{q}} + \frac{\upsilon * l_{org} * r_p}{4 * H_{org} * R * T * D_{org,eff} * r_{core}} \quad \text{(S3)}$$

Where α is the unitless accommodation coefficient (0.02), H_{inorg} is the Henry's law coefficient of IEPOX into the inorganic aqueous core of the aerosol particle (3×10^{-7} M/atm) that IEPOX dissolves in (Nguyen et al., 2014), D_a is the diffusivity of IEPOX into the inorganic aqueous portion of the aerosol particle (10^{-9} m^2/s), and q is the diffuso-reactive length represented by the following equation:

$$q = r_p\sqrt{\frac{k_{particle}}{D_a}} \quad \text{(S4)}$$

Where $k_{particle}$ is the pseudo-first-order rate constant (s^{-1}) represented by the following equation (Eddingsaas et al., 2010; Pye et al., 2013):

$$k_{particle} = \sum_{i=1}^{N}\sum_{j=1}^{M} k_{i,j}[nuc_i][acid_j] \quad \text{(S5)}$$

Where $k_{i,j}$ are individual acid-nucleophile rate constants defined by Supplemental Table 3.

When phase separation occurs r_{core} is calculated by the following equation (Schmedding et al., 2020):

$$l_{org} = r_p - r_{core} \quad \text{(S6)}$$

The first two terms of the γ_{IEPOX} reactive uptake probability equation (S3) represent that of an assumed homogeneously mixed aerosol. With assuming phase separation, a third term (the organic coatings resistor term) was added to this equation to represent the potential resistance to IEPOX reactive uptake in a phase-separated aerosol particle where l_{org} is the organic coating thickness, H_{org} is the Henry's Law coefficient dictating the dissolution of IEPOX into the organic coating (2×10^6 M/atm) (Zhang et al., 2018b), $D_{org,eff}$ is the diffusivity of IEPOX through organic coating (Fig 1, Eq. 7), and r_{core} is the radius of the inorganic aqueous core. When there is no phase separation l_{org} = 0, cancelling out the third resistor term and $r_{core} = r_p$ thus reverting equation S3 to the original parameterization of IEPOX reactive uptake currently in CMAQ.

Supplemental Table S1. For the saprctic07_ae7i chemical mechanism the aerosol species names, descriptions, anthropogenic (anth) or biogenic (biog) source, organic matter to organic carbon ratios ($OM{:}OC$) (Pye et al., 2017), atomic oxygen-to-carbon ratios ($O{:}C$) (Pye et al., 2017), molar mass (M) (Pye et al., 2017), saturation concentrations (C^0), hygroscopicity coefficients (k_{org}) (Petters et al., 2007), and predicted glass transition temperatures (T_g) with each parameterization (Li et al., 2020; Shiraiwa et al., 2017; Zhang et al., 2019b) found in Table 1.

Species Name	Description	Source	$OM{:}OC$	$O{:}C$	M (g/mol)	C^0 (µg/m3)	k_{org}	Predicted T_g (K) Shiraiwa	Predicted T_g (K) Zhang @ 298	Predicted T_g (K) Li

AAVB1	low volatility organic particulate matter from oxidation of anthropogenic VOCs (benzene, toluene, xylene, PAHs, alkanes)	anth	2.72	1.20	198.00	0.01	0.20	309.04	301.27	313.19
AAVB2	semivolatile organic particulate matter from oxidation of anthropogenic VOCs (benzene, toluene, xylene, PAHs, alkanes)	anth	2.27	1.10	179.00	1.00	0.15	289.57	264.55	289.10
AAVB3	semivolatile organic particulate matter from oxidation of anthropogenic VOCs (benzene, toluene, xylene, PAHs, alkanes)	anth	2.18	0.90	169.00	10.00	0.14	265.30	243.10	275.22
AAVB4	semivolatile organic particulate matter from oxidation of anthropogenic VOCs (benzene, toluene, xylene, PAHs, alkanes)	anth	2.00	0.60	158.00	100.00	0.12	229.71	219.46	258.82
ADIM	2-methyltetrol dimer	biog	2.07	0.74	248.23	0.0007	0.13	299.78	320.19	330.77

AGLY	Glyoxal / methylglyoxal SOA	biog	2.13	0.77	66.40	0.046	0.13	159.67	281.87	307.37
AIEOS	IEPOX-derived methyltetrol sulfate	biog	3.60	1.98	216.20	0.004	0.30	378.25	308.15	311.71
AIETET	2-methyltetrol	biog	2.27	0.88	136.15	0.46	0.15	238.65	268.74	293.59
AIMGA	2-methylglyceric acid	biog	2.50	1.10	120.10	22	0.18	247.08	232.08	271.21
AIMOS	methacrolein epoxide derived organosulfate	biog	4.17	2.40	200.16	0.056	0.36	408.04	288.77	299.57
AISO1	SV SOA product from isoprene	biog	2.20	0.81	132.00	116.01	0.14	228.04	216.02	259.22

AISO2	SV SOA product from isoprene	biog	2.23	0.85	133.00	0.62	0.15	232.68	266.15	291.97
AISOPNN	ISOP + NO3 organic nitrates	biog	3.80	2.12	226.00	8.65	0.32	391.74	247.22	279.80
AIVPO1	Intermediate Volatility Primary organic compounds	anth	1.17	0.01	266.00	1000.00	0.03	260.59	200.34	237.11
ALVOO1	LV Oxidized combustion organic compounds	anth	2.27	0.88	136.00	0.01	0.15	238.53	298.62	315.22
ALVOO2	LV Oxidized combustion organic compounds	anth	2.06	0.74	136.00	0.10	0.13	224.36	281.33	302.92
ALVPO1	LV Primary organic compounds	anth	1.39	0.16	218.00	0.10	0.05	238.94	285.02	304.80

AMT1	low volatility particulate matter from monoterpene photoxidation (OH and O3 reaction)	biog	1.63	0.38	300.00	0.01	0.08	299.62	304.15	318.51
AMT2	low volatility particulate matter from monoterpene photoxidation (OH and O3 reaction)	biog	1.63	0.38	200.00	0.10	0.08	243.02	284.36	304.10
AMT3	semivolatile particulate matter from monoterpene photoxidation (OH and O3 reaction)	biog	1.72	0.45	186.00	1.00	0.09	238.55	264.88	289.10
AMT4	semivolatile particulate matter from monoterpene photoxidation (OH and O3 reaction)	biog	1.54	0.30	184.00	10.00	0.07	224.59	243.91	273.29
AMT5	semivolatile particulate matter from monoterpene photoxidation (OH and O3 reaction)	biog	1.54	0.30	170.00	100.00	0.07	212.94	220.22	256.90
AMT6	semivolatile particulate matter from monoterpene photoxidation (OH and O3 reaction)	biog	1.36	0.16	168.00	1000.00	0.05	198.22	195.24	238.52

AMTHYD	organic pseudo-hydrolysis accretion product from monoterpene organic nitrates (AMTNO3J)	biog	1.54	0.30	186.00	53.23	0.07	226.20	227.80	261.58
AMTNO3	semivolatile organic nitrates from monoterpene oxidation	biog	1.90	0.59	231.00	12.00	0.11	280.27	244.34	273.03
AOLGA	Oligomer products of anthropogenic SOA compounds	anth	2.50	1.07	206.00	7.61	0.18	302.58	247.55	277.37
AOLGB	Oligomer products of biogenic SOA compounds	biog	2.10	0.74	248.00	2.63	0.13	299.67	258.95	283.13
AORGC	Cloud-formed SOA	biog	2.00	0.67	177.00	0.003	0.12	250.54	308.65	323.39
APCSO	Potential combustion SOA	anth	2.00	0.67	170.00	0.00001	0.12	245.27	341.74	353.58

APNCOM	Primary Combustion Non-carbon Organic Matter	anth	n/a	n/a	220.00	0.01	0.00	n/a	302.01	n/a
APOC	Primary Combustion Organic Carbon	anth	n/a	n/a	220.00	0.01	0.00	n/a	302.01	n/a
ASQT	SV SOA from sesquiterpenes	biog	1.52	0.30	273.00	24.98	0.07	283.10	238.91	266.84
ASVOO1	SV Oxidized combustion organic products	anth	1.88	0.59	135.00	85000.00	0.11	208.59	140.37	210.06
ASVOO2	SV Oxidized combustion organic products	anth	1.73	0.45	135.00	74000.00	0.09	195.09	142.06	208.94
ASVOO3	SV Oxidized combustion organic products	anth	1.60	0.38	134.00	63000.00	0.08	187.03	143.92	209.06

ASVPO1	SV primary organic compounds	anth	1.32	0.16	230.00	85000.00	0.05	247.44	146.84	203.23
ASVPO2	SV primary organic compounds	anth	1.26	0.08	241.00	74000.00	0.04	249.64	203.22	203.22
ASVPO3	SV primary organic compounds	anth	1.21	0.01	253.00	63000.00	0.03	252.47	203.42	203.42

Supplemental Table S2. The CMAQ species, noting if said species is lumped (L) or explicitly defined (E), their molecular formula, a suggested surrogate structure, their Simplified Molecular Input Line Entry System (SMILES) structure code, CMAQ molecular weights (M), and the OPEn structure–activity/property Relationship App (OPERA) estimated saturation concentration (C^0) values used for the Zhang and Li parameterizations. Cells in this table labeled N/A have values that already existed in the literature.

CMAQ Species (Explicit/Lumped)	**Molecular Formula CMAQ**	**Surrogate Chemical Structure**	**SMILES Structure**	**CMAQ M (g/mol)**	**OPERA C^0 (μg/m^3) (with CMAQ M)**
ADIM (L)	C10H16O7	(Pye et al., 2018) 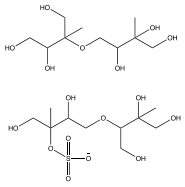	OCC(O)(C)C(O)COC(CO)(C)C(O)CO CC(O)(CO)C(CO)OCC(O)C(C)(CO)OS(=O)(=O)[O-]	248.2	0.0007

AORGC (L)	C7H13O5	(Loeffler et al., 2006) 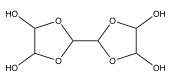	OC2OC(C1OC(O)C(O)O1)OC2O	177	0.003
AIEOS (E)	C5H12O7S	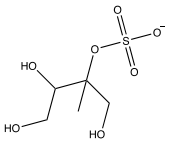	CC(CO)(OS(=O)(=O)[O-])C(O)CO	216.2	0.004
AIETET (E)	C5H12O4	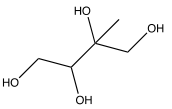	CC(O)(CO)C(O)CO	136.2	0.046
AIMGA (E)	C4H8O4	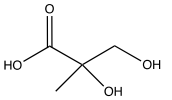	CC(O)(CO)C(=O)O	120.1	(Pye et al., 2018) 22
AIMOS (E)	C4H8O7S	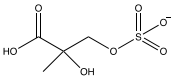	CC(O)(COS(=O)(=O)[O-])C(=O)O	200.2	0.056
AISOPNN (E)	C5H10O8N2	(Rollins et al., 2009) 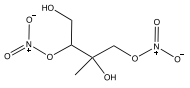	CC(O)(CON(=O)=O)C(CO)ON(=O)=O	226	8.65
AMTHYD (E)	C10H18O3	(Boyd et al., 2015)	CC1(C)C2CCC(CO)(OO)C1C2	186	52.23

		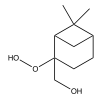			
AOLGA (L)	C7H10O7	N/A	N/A	206	(Pye et al., 2012) 7.61
AOLGB (L)	C10H16O7	N/A	N/A	248	(Sakulyanontvittaya et al., 2008) 2.627
AGLY (L)	C3O2 (-6 Hydrogens)	N/A	N/A	66.4	(Paciga et al., 2014) 0.046
APOC/APNCOM (L)	N/A	N/A	N/A	220	(Simon et al., 2012) 0.01

Supplemental Table S3. Individual third-order rate constants, $k_{i,j}$, for individual acid-catalyzed and nucleophilic addition reactions that produce IEPOX-SOA constituents (i.e., AIETET, AIEOS, and ADIM) per the saprc07tic_ae7i mechanism (Pye et al., 2017).

$k_{i,j}$	Value ($M^{-2}s^{-1}$)	Acid	Nucleophile	Product	Reference
k_{H^+,H_2O}	9×10^{-4}	H^+	H_2O	AIETET	(Eddingsaas et al., 2010; Pye et al., 2017; Pye et al., 2013)
$k_{H^+,SO_4^{2-}}$	1.27×10^{-3}	H^+	SO_4^{2-}	AIEOS	(Budisulistiorini et al., 2017; Riedel et al., 2016)

$k_{H^+,AIEOS}$	2×10^{-4}	H^+	AIEOS	ADIM	(Eddingsaas et al., 2010; Pye et al., 2017; Pye et al., 2013)
$k_{H^+,AIETET}$	2×10^{-4}	H^+	AIETET	ADIM	(Eddingsaas et al., 2010; Pye et al., 2017; Pye et al., 2013)
$k_{HSO_4^-,H_2O}$	1.31×10^{-5}	HSO_4^-	H_2O	AIETET	(Eddingsaas et al., 2010; Pye et al., 2017; Pye et al., 2013)
$k_{HSO_4^-,SO_4^{2-}}$	2.92×10^{-6}	HSO_4^-	SO_4^{2-}	AIEOS	(Eddingsaas et al., 2010; Pye et al., 2017; Pye et al., 2013)
$k_{HSO_4^-,AIEOS}$	2.92×10^{-6}	HSO_4^-	AIEOS	ADIM	(Eddingsaas et al., 2010; Pye et al., 2017; Pye et al., 2013)
$k_{HSO_4^-,AIETET}$	2.92×10^{-6}	HSO_4^-	AIETET	ADIM	(Eddingsaas et al., 2010; Pye et al., 2017; Pye et al., 2013)

65

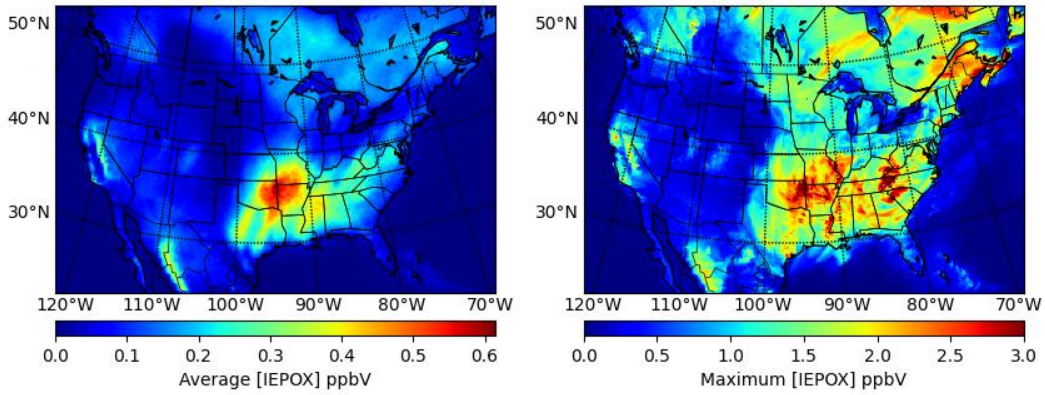

Supplemental Figure 1. Episode Averaged and Maximum IEPOX concentrations for the SOAS 2013 Field Campaign

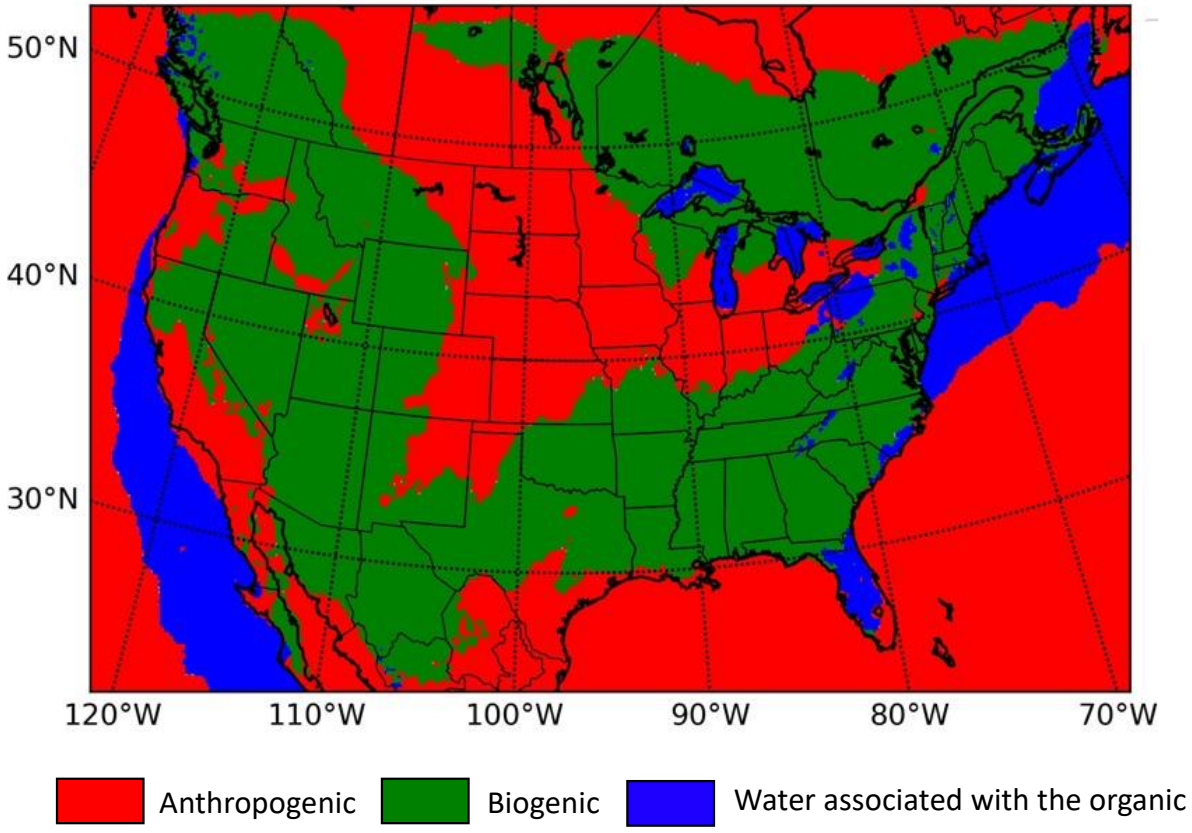

Supplemental Figure 2. Leading organic aerosol source to total organic aerosol shell mass.

70

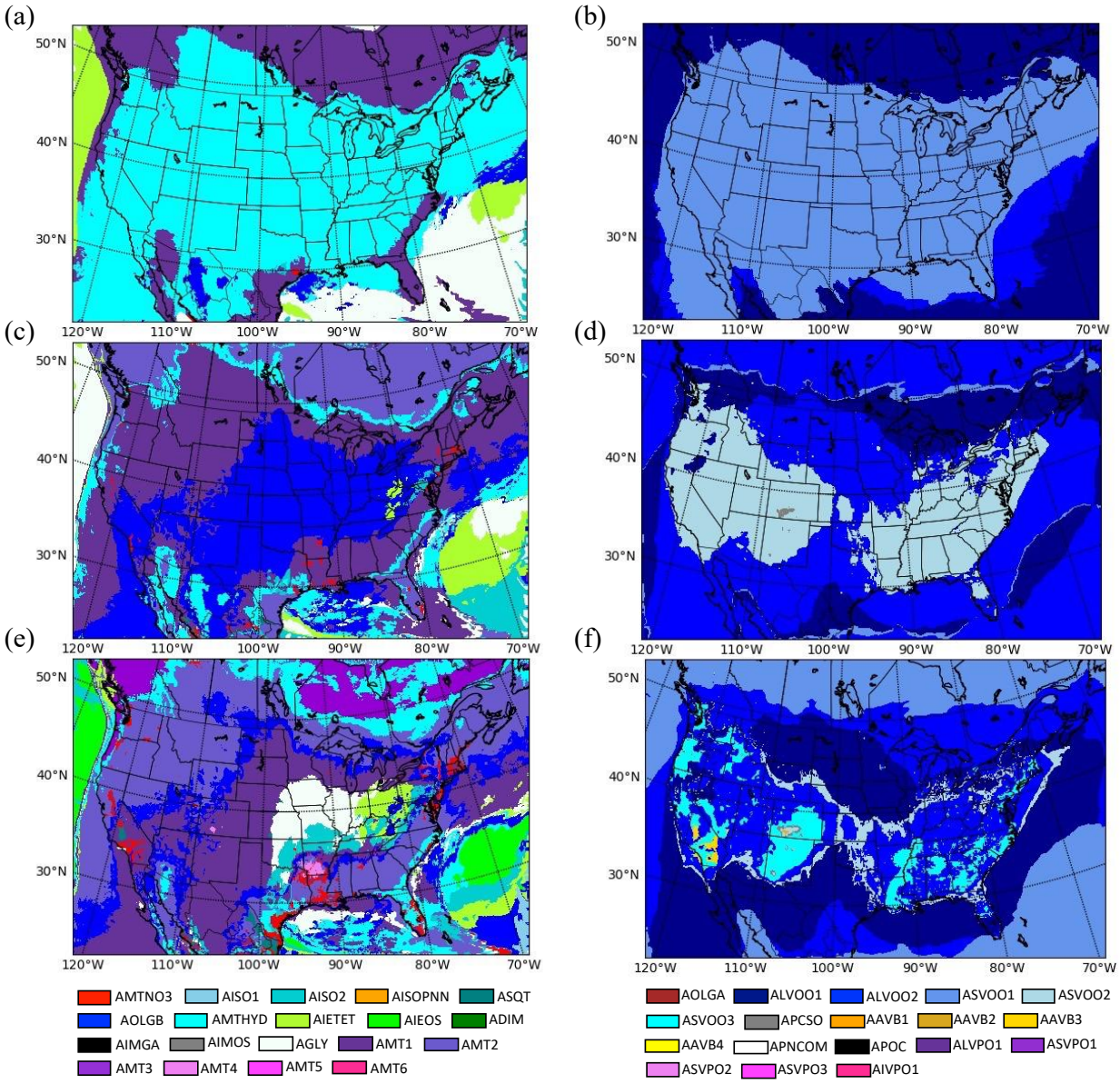

Supplemental Figure 3. The leading (a-b), second leading (c-d), and third leading (e-f) median aerosol concentration for each grid cell and across the simulation period of either total (a, c, & e) biogenic and (b, d, & f) anthropogenic species. Species names found in Supplemental Table S1.

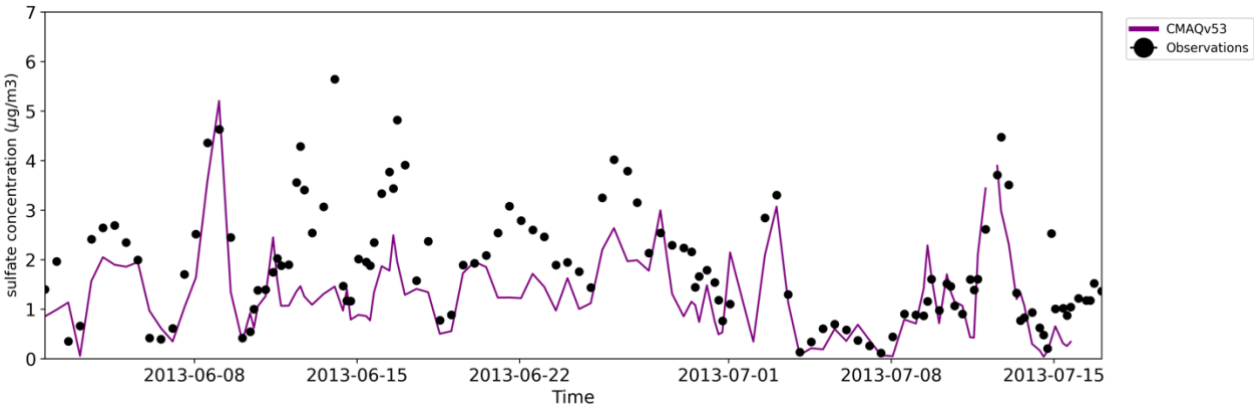

Supplementary Figure 4. Modeled and observed sulfate concentrations at the LRK SOAS site from June 1st to July 15th 2013.

References

Boyd, C. M., Sanchez, J., Xu, L., Eugene, A. J., Nah, T., Tuet, W. Y., Guzman, M. I., & Ng, N. L. Secondary organic aerosol formation from the β-pinene+NO₃ system: effect of humidity and peroxy radical fate. *Atmos. Chem. Phys., 15*(13), 7497-7522. doi:10.5194/acp-15-7497-2015 (2015).

Budisulistiorini, S. H., Nenes, A., Carlton, A. G., Surratt, J. D., McNeill, V. F., & Pye, H. O. T. Simulating Aqueous-Phase Isoprene-Epoxydiol (IEPOX) Secondary Organic Aerosol Production During the 2013 Southern Oxidant and Aerosol Study (SOAS). *Environmental Science & Technology, 51*(9), 5026-5034. doi:10.1021/acs.est.6b05750 (2017).

Eddingsaas, N. C., VanderVelde, D. G., & Wennberg, P. O. Kinetics and products of the acid-catalyzed ring-opening of atmospherically relevant butyl epoxy alcohols. *J Phys Chem A, 114*(31), 8106-8113. doi:10.1021/jp103907c (2010).

Gaston, C. J., Riedel, T. P., Zhang, Z., Gold, A., Surratt, J. D., & Thornton, J. A. Reactive Uptake of an Isoprene-Derived Epoxydiol to Submicron Aerosol Particles. *Environmental Science & Technology, 48*(19), 11178-11186. doi:10.1021/es5034266 (2014).

Li, Y., Day, D. A., Stark, H., Jimenez, J. L., & Shiraiwa, M. Predictions of the glass transition temperature and viscosity of organic aerosols from volatility distributions. *Atmos. Chem. Phys., 20*(13), 8103-8122. doi:10.5194/acp-20-8103-2020 (2020).

Loeffler, K. W., Koehler, C. A., Paul, N. M., & De Haan, D. O. Oligomer Formation in Evaporating Aqueous Glyoxal and Methyl Glyoxal Solutions. *Environmental Science & Technology, 40*(20), 6318-6323. doi:10.1021/es060810w (2006).

Nguyen, T. B., Coggon, M. M., Bates, K. H., Zhang, X., Schwantes, R. H., Schilling, K. A., Loza, C. L., Flagan, R. C., Wennberg, P. O., & Seinfeld, J. H. Organic aerosol formation from the reactive uptake of isoprene epoxydiols (IEPOX) onto non-acidified inorganic seeds. *Atmos. Chem. Phys., 14*(7), 3497-3510. doi:10.5194/acp-14-3497-2014 (2014).

Paciga, A. L., Riipinen, I., & Pandis, S. N. Effect of Ammonia on the Volatility of Organic Diacids. *Environmental Science & Technology, 48*(23), 13769-13775. doi:10.1021/es5037805 (2014).

Petters, M. D., & Kreidenweis, S. M. A single parameter representation of hygroscopic growth and cloud condensation nucleus activity. *Atmos. Chem. Phys., 7*(8), 1961-1971. doi:10.5194/acp-7-1961-2007 (2007).

Pye, H. O. T., Murphy, B. N., Xu, L., Ng, N. L., Carlton, A. G., Guo, H., Weber, R., Vasilakos, P., Appel, K. W., Budisulistiorini, S. H., Surratt, J. D., Nenes, A., Hu, W., Jimenez, J. L., Isaacman-VanWertz, G., Misztal, P. K., &

Goldstein, A. H. On the implications of aerosol liquid water and phase separation for organic aerosol mass. *Atmos. Chem. Phys., 17*(1), 343-369. doi:10.5194/acp-17-343-2017 (2017).

Pye, H. O. T., Pinder, R. W., Piletic, I. R., Xie, Y., Capps, S. L., Lin, Y.-H., Surratt, J. D., Zhang, Z., Gold, A., Luecken, D. J., Hutzell, W. T., Jaoui, M., Offenberg, J. H., Kleindienst, T. E., Lewandowski, M., & Edney, E. O. Epoxide Pathways Improve Model Predictions of Isoprene Markers and Reveal Key Role of Acidity in Aerosol Formation. *Environmental Science & Technology, 47*(19), 11056-11064. doi:10.1021/es402106h (2013).

Pye, H. O. T., & Pouliot, G. A. Modeling the Role of Alkanes, Polycyclic Aromatic Hydrocarbons, and Their Oligomers in Secondary Organic Aerosol Formation. *Environmental Science & Technology, 46*(11), 6041-6047. doi:10.1021/es300409w (2012).

Pye, H. O. T., Zuend, A., Fry, J. L., Isaacman-VanWertz, G., Capps, S. L., Appel, K. W., Foroutan, H., Xu, L., Ng, N. L., & Goldstein, A. H. Coupling of organic and inorganic aerosol systems and the effect on gas–particle partitioning in the southeastern US. *Atmos. Chem. Phys., 18*(1), 357-370. doi:10.5194/acp-18-357-2018 (2018).

Riedel, T. P., Lin, Y. H., Zhang, Z., Chu, K., Thornton, J. A., Vizuete, W., Gold, A., & Surratt, J. D. Constraining condensed-phase formation kinetics of secondary organic aerosol components from isoprene epoxydiols. *Atmos. Chem. Phys., 16*(3), 1245-1254. doi:10.5194/acp-16-1245-2016 (2016).

Rollins, A. W., Kiendler-Scharr, A., Fry, J. L., Brauers, T., Brown, S. S., Dorn, H. P., Dubé, W. P., Fuchs, H., Mensah, A., Mentel, T. F., Rohrer, F., Tillmann, R., Wegener, R., Wooldridge, P. J., & Cohen, R. C. Isoprene oxidation by nitrate radical: alkyl nitrate and secondary organic aerosol yields. *Atmos. Chem. Phys., 9*(18), 6685-6703. doi:10.5194/acp-9-6685-2009 (2009).

Sakulyanontvittaya, T., Guenther, A., Helmig, D., Milford, J., & Wiedinmyer, C. Secondary Organic Aerosol from Sesquiterpene and Monoterpene Emissions in the United States. *Environmental Science & Technology, 42*(23), 8784-8790. doi:10.1021/es800817r (2008).

Schmedding, R., Ma, M., Zhang, Y., Farrell, S., Pye, H. O. T., Chen, Y., Wang, C.-T., Rasool, Q. Z., Budisulistiorini, S. H., Ault, A. P., Surratt, J. D., & Vizuete, W. α-Pinene-Derived Organic Coatings on Acidic Sulfate Aerosol Impacts Secondary Organic Aerosol Formation from Isoprene in a Box Model. *Atmospheric environment (Oxford, England : 1994), 213*, 456-462. doi:10.1016/j.atmosenv.2019.06.005 (2019).

Schmedding, R., Rasool, Q. Z., Zhang, Y., Pye, H. O. T., Zhang, H., Chen, Y., Surratt, J. D., Lopez-Hilfiker, F. D., Thornton, J. A., Goldstein, A. H., & Vizuete, W. Predicting secondary organic aerosol phase state and viscosity and its effect on multiphase chemistry in a regional-scale air quality model. *Atmos. Chem. Phys., 20*(13), 8201-8225. doi:10.5194/acp-20-8201-2020 (2020).

Shiraiwa, M., Li, Y., Tsimpidi, A. P., Karydis, V. A., Berkemeier, T., Pandis, S. N., Lelieveld, J., Koop, T., & Pöschl, U. Global distribution of particle phase state in atmospheric secondary organic aerosols. *Nature Communications, 8*(1), 15002. doi:10.1038/ncomms15002 (2017).

Simon, H., & Bhave, P. V. Simulating the Degree of Oxidation in Atmospheric Organic Particles. *Environmental Science & Technology, 46*(1), 331-339. doi:10.1021/es202361w (2012).

Zhang, Y., Chen, Y., Lambe, A. T., Olson, N. E., Lei, Z., Craig, R. L., Zhang, Z., Gold, A., Onasch, T. B., Jayne, J. T., Worsnop, D. R., Gaston, C. J., Thornton, J. A., Vizuete, W., Ault, A. P., & Surratt, J. D. Effect of the Aerosol-Phase State on Secondary Organic Aerosol Formation from the Reactive Uptake of Isoprene-Derived Epoxydiols (IEPOX). *Environmental Science & Technology Letters, 5*(3), 167-174. doi:10.1021/acs.estlett.8b00044 (2018b).

Zhang, Y., Nichman, L., Spencer, P., Jung, J. I., Lee, A., Heffernan, B. K., Gold, A., Zhang, Z., Chen, Y., Canagaratna, M. R., Jayne, J. T., Worsnop, D. R., Onasch, T. B., Surratt, J. D., Chandler, D., Davidovits, P., & Kolb, C. E. The Cooling Rate- and Volatility-Dependent Glass-Forming Properties of Organic Aerosols Measured by Broadband Dielectric Spectroscopy. *Environmental Science & Technology, 53*(21), 12366-12378. doi:10.1021/acs.est.9b03317 (2019b).